HHS Public Access
Author manuscript
Exp Math. Author manuscript; available in PMC 2015 September 29.

Published in final edited form as:
Exp Math. 2014 ; 23(4): 465–474. doi:10.1080/10586458.2014.947053.

Fingering in Stochastic Growth Models

Andreas C. Aristotelous and **Richard Durrett***
Department of Mathematics, Duke U., Box 90320, Durham, NC 27708-0320

Abstract

Motivated by the widespread use of hybrid-discrete cellular automata in modeling cancer, two simple growth models are studied on the two dimensional lattice that incorporate a nutrient, assumed to be oxygen. In the first model the oxygen concentration $u(x, t)$ is computed based on the geometry of the growing blob, while in the second one $u(x, t)$ satisfies a reaction-diffusion equation. A threshold θ value exists such that cells give birth at rate $\beta(u(x, t) - \theta)^+$ and die at rate $\delta(\theta - u(x, t)^+$. In the first model, a phase transition was found between growth as a solid blob and "fingering" at a threshold $\theta_c = 0.5$, while in the second case fingering always occurs, i.e., $\theta_c = 0$.

1 Introduction

Stochastic growth models have a long history. Eden [10] introduced a model on the d-dimensional square lattice $\mathbb{Z}^d$ in which there are occupied and vacant sites. (i) Once a site is occupied it stays occupied forever, and (ii) a site with k of its nearest neighbors occupied becomes occupied at rate $k/2d$. A dozen years later, Richardson [28] was the first to show that if we start Eden's model from only the origin occupied, then the set of occupied sites at time t, ξ_t grows linearly and has an asymptotic shape.

Shape Theorem

There is a convex set D with the same symmetries as $\mathbb{Z}^d$ so that for any $\varepsilon > 0$ there is a $t_0(\varepsilon)$ so that for $t \geq t_0(\varepsilon)$

$$(1-\varepsilon)tD \cap \mathbb{Z}^d \subset \xi_t \subset (1+\varepsilon)tD.$$

The key observation in proving this was that the occupation times were "subadditive." To explain let us reformulate the model as first passage percolation. See [29, 5, 20]. Associated with each edge e is an exponential random variable $X(e)$ with rate $1/2d$, which we think of as the time for a fluid to traverse the edge. Given sites x and y, the first passage time $t(x, y)$ is the minimum of $X(e_1) + \cdots X(e_k)$ over all paths from x to y. It is not hard to check that if we let $\eta_t = \{x : t(0, x) = t\}$ then η_t is Eden's growth model.

The passage times have the property that

*These authors were partially supported by NIH grant 5R01GM096190.

$$t(x,z) \le t(x,y)+t(y,z).$$

From this Richardson was able to show that if e_1 is the first unit vector then

$$t(0,ne_1)/n \to \inf_{n\ge 1} Et(0,ne_1)/n. \quad (1)$$

Once this is established it is not hard to prove the Shape Theorem. The argument for (1) was generalized by Kingman [23] to become his subadditive ergodic theorem, which is a useful tool in many situations, see Section 7.4 in [9].

At about the time of Richardson's work, Williams and Bjerknes [31] introduced a simple spatial model for the spread of cancer. Each site on the square lattice is occupied by a normal cell (state 0) or a cancer cell (state 1). Let $n_i(x)$ be the number of neighbors of x in state i. Sites in state 1 become state 0 at rate $n_0(x)/4$, and sites in state 0 become state 1 at rate $\lambda n_1(x)/4$. In the field of interacting particle systems, this is called the biased voter model. Bramson and Griffeath [4, 3] used subadditivity results to show that the conclusion of the shape theorem held for the biased voter model.

The biased voter model, also known as the spatial Moran model, is simple, but is useful as a cancer model because it is possible to prove a number of results about its asymptotic behavior. The last half-dozen years have seen the use of complex spatial cancer models that explicitly model nutrient concentrations which govern the birth and death rates of the cells which produce and absorb them, and diffuse according to partial differential equations. Such models often take place on a lattice, [12, 1, 14, 15], but in some cases, the cells have a size and shape and interact through mechanical forces. See e.g., [6, 8, 25, 27] for examples, or [2, 8, 26] for surveys that contrast the different styles of modeling.

These complex models can only be studied by simulation. To begin to build a theory for predicting their behavior, we take the simple first step of adding one nutrient, oxygen, to the Richardson's model described above, and have the birth and death rates of cells depend on their oxygen levels. Our models will have empty sites ($\xi_t(x) = 0$) cancer cells ($\xi_t(x) = 1$), and dead cancer cells ($\xi_t(x) = -1$). Our first model will be static, i.e., the oxygen level at a site will be computed based on the states of nearby sites. Our second model will include diffusion of oxygen and its absorption by living cells.

2 Static Model

We have a two dimensional lattice in a finite square domain Ω. To define the dynamics we let $|z|=(z_1^2+z_2^2)^{1/2}$ be the usual Euclidean distance and define

$$u(x,t)=\frac{1}{R_{max}}\left(\sum_{y\neq x} e^{-\lambda|y-x|}1_{(\xi_t(y)=0)}\right) \quad (2)$$

where $R_{\max}$ is the maximum value of the sum

$$R_{max}=\sum_{x\neq 0} e^{-\lambda|x|} \quad (3)$$

and the parameter $\lambda > 0$ dictates the scale $O(1/\lambda)$, of the interaction.

Let θ be the amount of oxygen needed for the cell to survive and let $\Phi(x, t) = u(x, t) - \theta$. Cells with $\Phi(x, t) > 0$ give birth at rate $\beta\Phi(x, t)$ while those with $\Phi(x, t) < 0$ die at rate $-\delta\Phi(x, t)$. To simulate this continuous time Markov chain, we select a site at random from the set of sites occupied by a living cancer cell. The maximum rate at which changes can occur is $\Gamma = \max\{\beta(1 - \theta), \delta\theta\}$. If $\Phi(x, t) < 0$ the cell dies with probability $-\delta\Phi(x)/\Gamma$. If $\Phi(x, t) > 0$ then a birth occurs with probability $\beta\Phi(x, t)/\Gamma$ and the offspring is sent to one of the four nearest neighbors. If that site is occupied then nothing happens.

2.1 Simulations

To show what the process does, Figure 1 simulates the system with $\lambda = 0.05$, $\beta = 0.8$, and $\delta = 1$ for $\theta = 0.1, 0.2, \ldots, 0.6$. We start the simulations with one living cancer cell centrally located and we perform ten million site updates. Depending on the value of θ this produces a blob with radius 150–200. When $\theta = 0.1, 0.2$ the growing blob is roughly circular, although in the second case one can see that when a large crevice occurs, the cells deep within it do not have enough oxygen and their growth stops.

When $\theta > 0.5$, the system cannot grow like Eden's model, because if the blob is exactly a ball and the ball is large, then points along the boundary would not have enough oxygen to grow. Of course, the shape is never exactly a ball, but when the radius of the blob is large, the points that are lagging behind the edge of the front have even less oxygen and cannot grow. The simulations show that when $\theta = 0.5, 0.6$ the growing blob is not solid but has permanent fjords of 0's. In this case we say that fingering occurs, or to be precise, we make

> **Conjecture 1.** *If $\theta > 0.5$ then there is at least one point x_0 so that for all t, $\xi_t(x_0) = 0$, and x_0 is connected to ∞ by a path of sites y with $\xi_t(y) = 0$.*

The existence of x_0 implies that there will be at least one permanent fjord. We expect that the number of fjords will grow linearly with time, but it is not easy to explain precisely how to count the them.

The conjectured behavior for $\theta > 0.5$ is reminiscent of the behavior of diffusion limited aggregation (DLA). To quote Witten and Sandler [34],“ DLA is an idealization of the process by which matter irreversibly combines to form dust, soot, dendrites, and other random objects in the case where the rate-limiting step is diffusion of matter to the aggregate.” The rules of the model are quite simple. We start with a cluster that consists of a single particle at the origin of a lattice. Once we have a cluster of size *n*, another particle starts a random walk from a site that is “far away” from the growing cluster, which in practice means at a point chosen uniformly at random on a circle that is large enough to enclose the cluster. This particle walks until it arrives at one of the lattice sites adjacent to an occupied site. It is added to the cluster and another particle is launched. For a simulation see

Figure 2. The picture may remind the reader of electrical discharge. Indeed, the dielectric breakdown that occurs when the voltage applied to a solid exceeds the breakdown voltage produce DLA-like patterns called Lichtenburg figures, see [30]. Similar growth can be seen in a number of situations such as zinc metal leaves grown by electrodeposition [24], or the viscous fingering that occurs when a low viscosity fluid is forced into a high-viscosity liquid [7].

The paper [34] which defined DLA has been cited more than 1100 times, according to Science Citation Index, but as far as we know, the only rigorous results in two dimensions are those of Kesten [21, 22] who showed that the arms asymptotically grew at most at rate $n^{2/3}$. There has been a large amount of numerical work, and the fractal dimension has been estimated to be 1.7. See [17] for this and references to the literature. Note that the arms of DLA in Figure 2 are much thinner than those in our simulation of $\theta = 0.6$. In our process the arms will thicken until the oxygen contributions are no longer sufficient for growth to continue. Figure 3 shows our model with $\theta = 0.7, 0.8$ run for twenty million updates. The pictures are now similar to the one for DLA.

When $\theta = 0.3$, crevices form but then later the boundaries connect, resulting in trapped regions in state 0. The reconnection does not happen for $\theta = 0.4$ in Figure 1. However, when we simulate $\theta = 0.4, 0.45$ for longer time (see Fig. 4), we observe that again the boundaries come together. Based on this, we make

Conjecture 2. *Let ζ_t be the collection of sites x at time t where $\xi_t(x) = -1$ or $\xi_t(x) = 0$ and x is in a bounded component of sites in state 0. The shape theorem holds for ζ_t when $\theta < 0.5$.*

3 Oxygen Diffusion Model

Now we consider a more realistic model in which the oxygen diffuses and is absorbed by living cells. The oxygen concentration at x at time t, $u(x, t)$, is modeled by the following reaction diffusion PDE,

$$\frac{\partial u}{\partial t} = D\Delta u - \mu 1_{(\xi(x)=1)}\, u. \quad (4)$$

As in the previous model, the transition rates depend on $\Phi(x, t) = u(x, t) - \theta$. Cells with $\Phi(x, t) > 0$ give birth at rate $\beta\Phi(x, t)$ while those with $\Phi(x, t) < 0$ die at rate $-\delta\Phi(x, t)$. To simulate the system, we use a square domain Ω, with Dirichlet boundary conditions, $u = u_0$, on the boundary $\partial\Omega$. To have a faithful simulation of the system on the infinite lattice, we stop the growth before the blob gets close to the boundary of the square domain Ω.

We start the simulation with one cell initially and $u(x, 0) = u_0(x)$. To numerically solve the initial boundary value problem in (4) describing the chemical dynamics we use a two dimensional square lattice with spacing, $h \ll 1$, between neighboring lattice nodes. For the temporal discretization of (4) we employ the modified Euler [33] method, which is of second order in time and can be written as an explicit Runge-Kutta. In the examples here, $D = 0.1$ and a stable time step $\tau = 0.001$ was used.

In order to simulate the birth and death events, we use a discrete time approximation with time step $\tau_s > \tau$, which in most cases is $\tau_s = 0.1$. Assuming $\Phi(x, t) > 0$, a living cancer cell occupying a node x gives birth on a randomly selected nearest neighbor node with probability $\tau_s \beta \Phi(x, t)$, if the selected neighbor is vacant. Similarly if $\Phi(x, t) < 0$ the cell dies with probability $-\tau_s \delta \Phi(x, t)$. Note that we do births and deaths once for every 100 PDE updates. This is done to reduce the amount of work, while keeping the number of collisions (i.e., situations in which a site and its neighbor are both updated in one iteration) relatively small, so we have an accurate approximation of the continuous time process.

3.1 Simulation results

In Figures 5 we fix all the parameters $D = 0.1$, $\mu = 0.125$, $\beta = 1.2$, and $\delta = 0.4$ and look at the behavior for $\theta = 0.1, \ldots 0.6$. The domain is 400×400 and we run the simulation, until the growing blob exits the square centered at the origin with side 240. As the reader might expect from the static case, fingering occurs for $\theta = 0.5, 0.6.$, while the system is like a blob for $\theta = 0.1, 0.2$. However, now when we run the simulation for longer for $\theta = 0.2, 0.3$ in Figure 6 we observe that fingering eventually develops. Based on this observation we make

> **Conjecture 3.** *If $\theta > 0$ then there is at least one point x_0 so that for all t, $\xi_t(x_0) = 0$, and x_0 is connected to ∞ by a path of sites y with $\xi_t(y) = 0$.*

To further investigate the reason why the system never grows like a solid blob, we start the simulation with a ball of radius $r = 100$, in a 800×800 domain, with living cells only along a thin layer from the boundary for $\theta = 0.2$, keeping the same parameters as before. In Figure 7 we see that a radially symmetric initial condition maintains its symmetry for a while (panels a and b) but then the symmetry breaks down (panels d and e). Intuitively this is due to the fact that the circle is not stable: if part of the boundary gets ahead due to stochastic effects then it grows faster, while parts of the boundary that get behind, fall further behind.

Our system has some elements in common with motion by mean-curvature, in which one allows a surface to evolve by moving each point at velocity equal to the mean curvature vector at that point. This process is delicate to study in $d > 2$, see Evans and Spruck [11], but can be handled by more elementary methods in $d = 2$. See Gage and Hamilton [13] for the case of a convex initial curve or Grayson [16] for a smooth one. The main result as stated in the title of [16] is that the flow "shrinks embedded plane curves to round points." To be precise, the curve shrinks to a point as $t \to \infty$ and its limiting shape is that of a circle.

In contrast, a PDE version of our model could be defined without using differential geometry as follows. Parametrize the boundary so that it is traversed at unit speed. Given a point on the boundary rotate the solid so that the tangent to the curve is horizontal and the interior lies below. Let $\kappa(x)$ be the second derivative of the height at the point x. We declare that growth stops at points where the curvature $\kappa(x) > \theta$, and motion occurs in the direction of the outward pointing normal vector at speed $\beta(\kappa(x) - \theta)$. However, to have a good analogy one would have to introduce smooth stochastic fluctuations at the boundary. One way to find an appropriate continuum model would be to take a scaling limit of our particle system. Katsoulakis and Souganidis, and others, see [19] for details and references, have shown that under rescaling interfaces in a long range version of the Ising model converge to

motion by mean curvature. However, formulating and proving such a result for our system seems very difficult.

4 Conclusions

We have investigated two models with a nutrient whose level $u(x, t)$ dictates the rate of growth $\beta(u(x, t) - \theta)^+$ or of death $\delta(\theta - u(x, t))^+$. In first case, we find a phase transition between growth as a solid blob and "fingering" at a threshold $\theta_c = 0.5$, while in the second case fingering always occurs, i.e., $\theta_c = 0$.

We believe that this difference in behavior can be traced to the space scales involved. In the first (static) model the nutrient concentration at a cell is calculated by considering only vacant nodes within the support of a nutrient kernel (2), centered at that cell. In this case, there is a fixed radius of interaction, so sites separated by more than that distance evolve independently. Because of this, the size of disturbances stays constant.

In the case of the second (diffusion) model, oxygen is being introduced from the boundary and diffuses in the domain being partially absorbed by living cancer cells, so the length scale over which the nutrient levels vary is proportional to the the size of the blob. Because of this, a solid blob is subject to a destabilizing disturbance with probability independent of its size and eventually succumbs.

Here, we have concentrated on the behavior of the two models as a mathematical puzzle: what growth rules result in fingering rather than growth as a solid blob. There is also the related question: what biological mechanisms promote fingering. Is it due to cell adhesion [1] or hypoxia [12] which is the driver in our models. Answering the last question is important if one wants, as [25] suggest, to use tumor morphology to predict the efficiency of antiangiogenic therapy. More generally, one must have an understanding of the mechanisms at work in complex hybrid-discrete cellular automata if one wants to use them to assess chemotherapy strategies, [18].

References

1. Anderson ARA. A hybrid mathematical model of solid tumor invasion: the importance of cell adhesion. Mathematical Medicine and Biology. 2005; 22:163–186. [PubMed: 15781426]
2. Anderson ARA, Rejniak KA, Gerlee P, Quaranata V. Modeling of cancer growth, evolution, and invasion: Bridging scales and models. Math Model Nat Phenom. 2007; 2:1–29.
3. Bramson M, Griffeath D. On the Williams-Bjerknes tumour growth model. II. Math Proc Cambridge Philos Soc. 1980; 88:339–357.
4. Bramson M, Griffeath D. On the Williams-Bjerknes tumour growth model. I. Ann Probab. 1981; 9:173–185.
5. Cox JT, Durrett R. Some limit theorems for first passage percolation with necessary and sufficient conditions. Ann Prob. 1981; 9:583–603.
6. Cristini, V.; Lowengrub, J. Multiscale Modeling of Cancer. Cambridge U. Press; 2010.
7. Daccord G, Nittmaann J, Stanley HE. Radial viscous fingers and diffusion-limited aggregation: fractal dimension and growth sites. Physical Review Letters. 1986; 56:336–339. [PubMed: 10033161]
8. Deisboeck TS, Wang Z, Macklin P, Cristini V. Multiscale cancer modeling. Annual Rev Biomed Eng. 2011; 13:127–155. [PubMed: 21529163]

9. Durrett, R. Probability: Theory and Examples. 4. Cambridge U. Press; 2010.
10. Eden, M. Proceedings of Fourth Berkeley Symposium on Mathematics, Statistics, and Probability. Vol. 4. University of California Press; Berkeley: 1961. A two-dimensional growth process; p. 223-239.
11. Evans LC, Sprcuk J. Motion of level sets by mean curvature, I. J Diff Geo. 1991; 33:635–681.
12. Ferreira SC, Martins ML, Viela MJ. Reaction-diffusion model for the growth of an avascular tumor. Physical Review E. 2002; 65:paper 021907.
13. Gage M, Hamilton RS. The heat equation shrinking plane curves. J Diff Geo. 1986; 23:69–96.
14. Gerlee P, Anderson ARA. An evolutionary hybrid cellular automation model of solid tumor growth. J Theoretical Biology. 2007; 246:583–603.
15. Gerlee P, Anderson ARA. A hybrid cellular automaton model of clonal evolution in cancer: The emergence of the glycolytic phenotype. J Theoretical Biology. 2008; 250:705–722.
16. Grayson MA. The heat equation shrinks curves to round points. J Diff Geo. 1987; 26:285–314.
17. Hastings Matthew B. Renormalization theory of stochastic growth. Physical Review E. 1997; 55:135–152.
18. Hinow P, et al. A spatial model of tumor-host interaction: Application to chemotherapy. Math Biosci Engr. 2009; 6:521–546.
19. Katsoulakis MA, Souganidis PE. Generalzied motion by mean curvature as a macroscopic limit of stochastic Ising models with long range interactions and Glauber dynamics. Commun Math Phys. 1995; 169:61–97.
20. Kesten H. Aspects of first passage percolation. Springer Lecture Notes in Math 1180. 1986
21. Kesten H. How long are the arms of DLA? Journal of Physics A. 1987; 20:L29–L33.
22. Kesten H. Upper bounds on the growth rate of DLA. Physica A. 1990; 168:529–535.
23. Kingman JFC. Subadditive ergodic theory. Ann Probab. 1973; 1:883–909.
24. Matsushita M, Sano M, Hayakawa Y, Honjo H, Sawada Y. Fractal structure of zinc metal leaves grwon by electrodeposition. Physical Review Letters. 1984; 53:286–289.
25. Poplawski NJ, Agero U, Gens JG, Swat M, Glazier JA, Anderson ARA. Front instabilities and invasiveness of simulated avascular tumors. Bulletin of Mathamtical Biology. 2009; 71:1189–1227.
26. Quaranta V, Rejniak KA, Gerlee P, Anderson ARA. Invasion emerges from cancer cell adaptation to competitive microenvironments: Quantitative predictions from multi-scale mathematical models. Seminars in Cancer Biology. 2008; 18:338–348. [PubMed: 18524624]
27. Rejniak KA, Anderson ARA. Hybrid models of tumor growth. Systems Biology and Medicine. 2011; 3:115–125. [PubMed: 21064037]
28. Richardson D. Random growth in a tesselation. Proc Camb Phil Soc. 1973; 74:515–528.
29. Smythe, R.; Weirman, JC. First Passage Percolation on the Square Lattice. Springer; 1977. Lecture Notes in Math 671
30. Takahashi Y. Two Hundred Years of Lichtenberg Figures. Journal of Electrostatics. 1979; 6:1–13.
31. Williams T, Bjerknes R. Stochastic model for abnormal clone spread through epithelial basal layer. Nature. 1972; 235:19–21. [PubMed: 4553633]
32. Liggett, TM. Interacting Particle Systems. Springer-Verlag; New York, NY: 1985.
33. Süli, E.; Mayers, D. An Introduction to Numerical Analysis. Cambridge U. Press; 2003.
34. Witten TA, Sandler LM. Diffusion limited aggregation. Phys Rev B. 1983; 27:5686–5697.

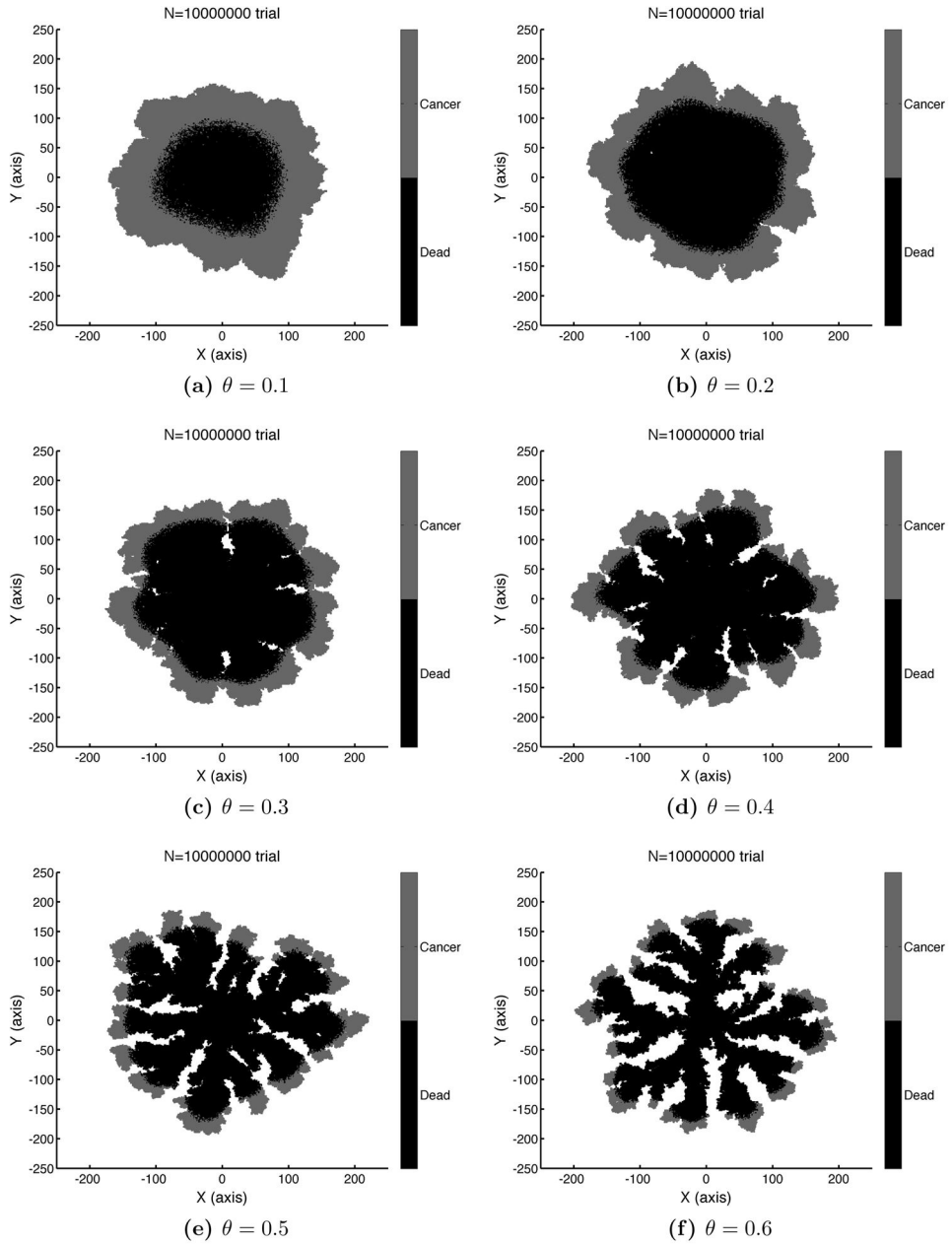

Figure 1.

Simulation snapshots for the static model. Parameters $\lambda = 0.05$, $\beta = 0.8$, $\delta = 1$ and $\theta = 0.1, \ldots, 0.6$. The final profile of the model evolution is depicted for each case where black indicates dead cancer cells, gray indicates living cancer cells and white is empty space.

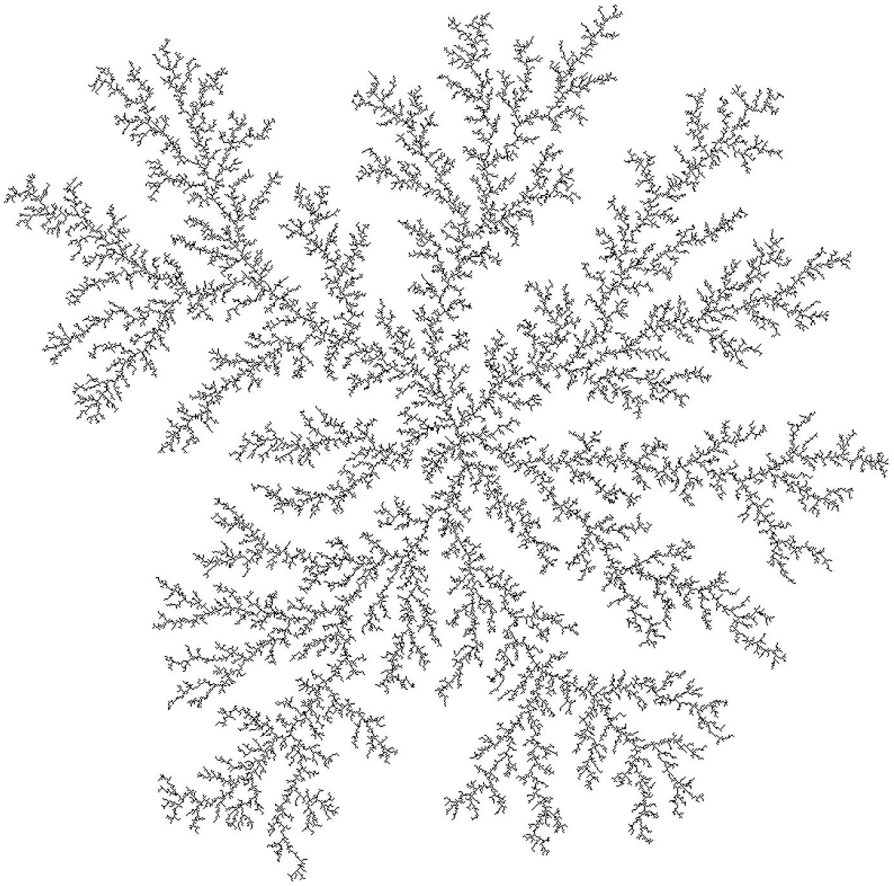

Figure 2.
Simulation snapshot of a DLA model.

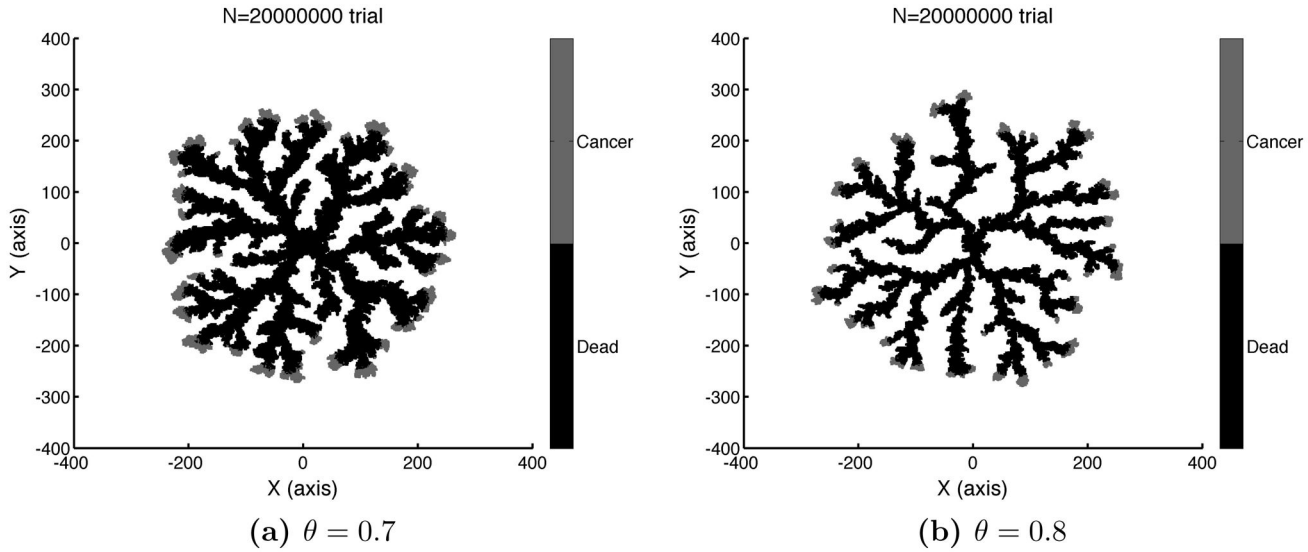

(a) $\theta = 0.7$ (b) $\theta = 0.8$

Figure 3.

Simulation snapshots for the static model for $\theta = 0.7$ and $\theta = 0.8$. The final profile of the model evolution for 20 million trials is depicted corresponding to each case. Parameters and color scheme as in Figure 1.

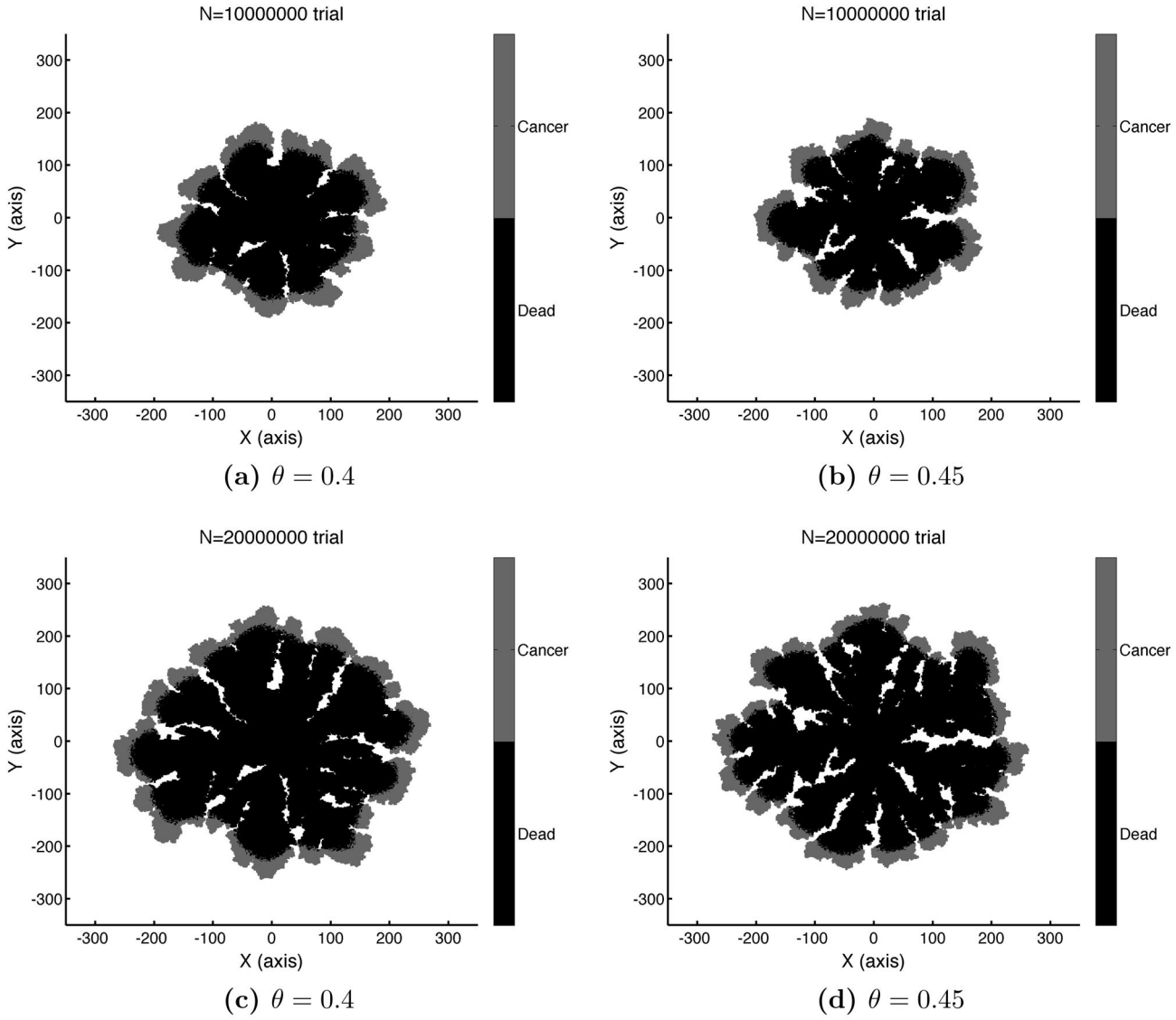

Figure 4.

Simulation snapshots for the static model. At the first column $\theta = 0.4$ and at the second $\theta = 0.45$. The final profile of the model evolution for 10 and 20 million trials is depicted corresponding to each θ case. Parameters and color scheme as in Figure 1.

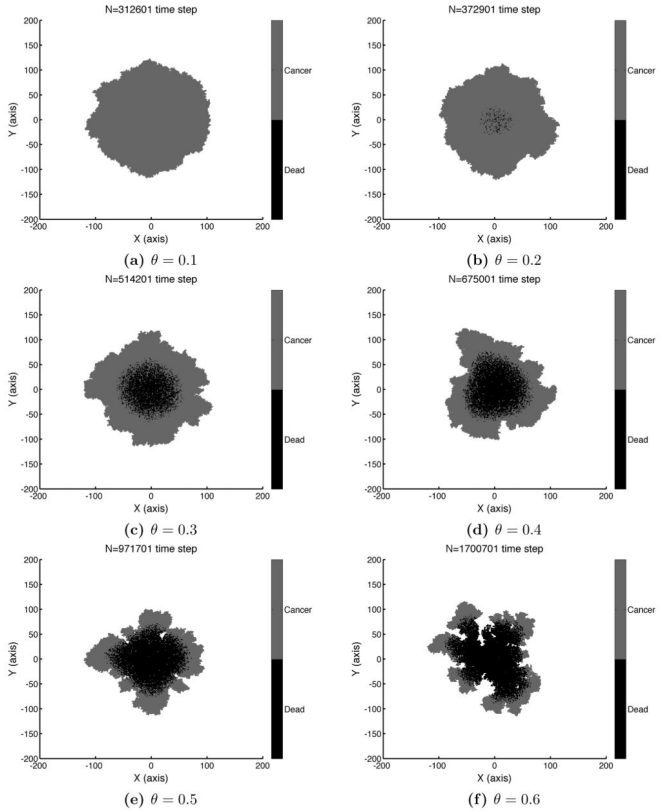

(a) $\theta = 0.1$ (b) $\theta = 0.2$ (c) $\theta = 0.3$ (d) $\theta = 0.4$ (e) $\theta = 0.5$ (f) $\theta = 0.6$

Figure 5.

Simulation snapshots using the diffusive model. Here we have plotted for each of the following values of the parameter $\theta = 0.1, 0.2, 0.3, 0.4, 0.5, 0.6$ the model evolution where black indicates dead cancer cells, while gray indicates living cancer cells. The other model parameters are: birth coefficient $\beta = 1.2$, death coefficient $\delta = 0.4$, $D = 0.1$ and $\mu = 0.125$ fixed. We used $\tau_s = 0.1$ and $\tau = 0.001$. Our computational domain's Ω actual size is 400×400. In each case we have started the simulation by using one living cancer cell located in the center of Ω, and run the simulation until the growing blob reached the boundary of the inner centered square with side length 240.

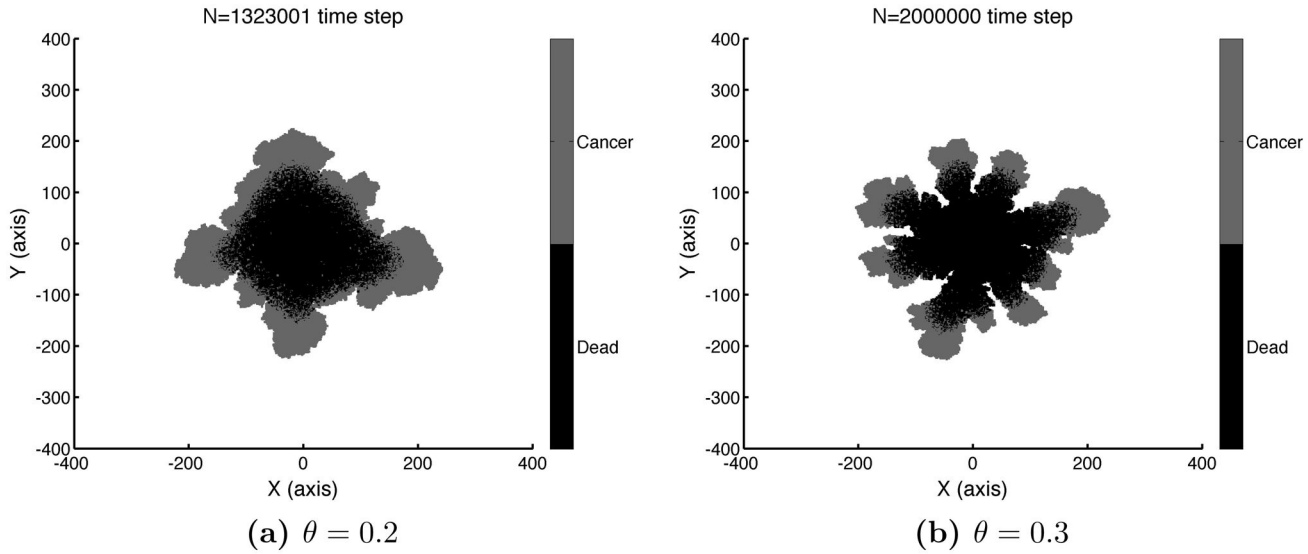

(a) $\theta = 0.2$ (b) $\theta = 0.3$

Figure 6.

Simulations of $\theta = 0.2$, and 0.3 on an 800 × 800 square stopped when the process has escaped the square with radius 480. Parameters and color scheme as in Figure 5.

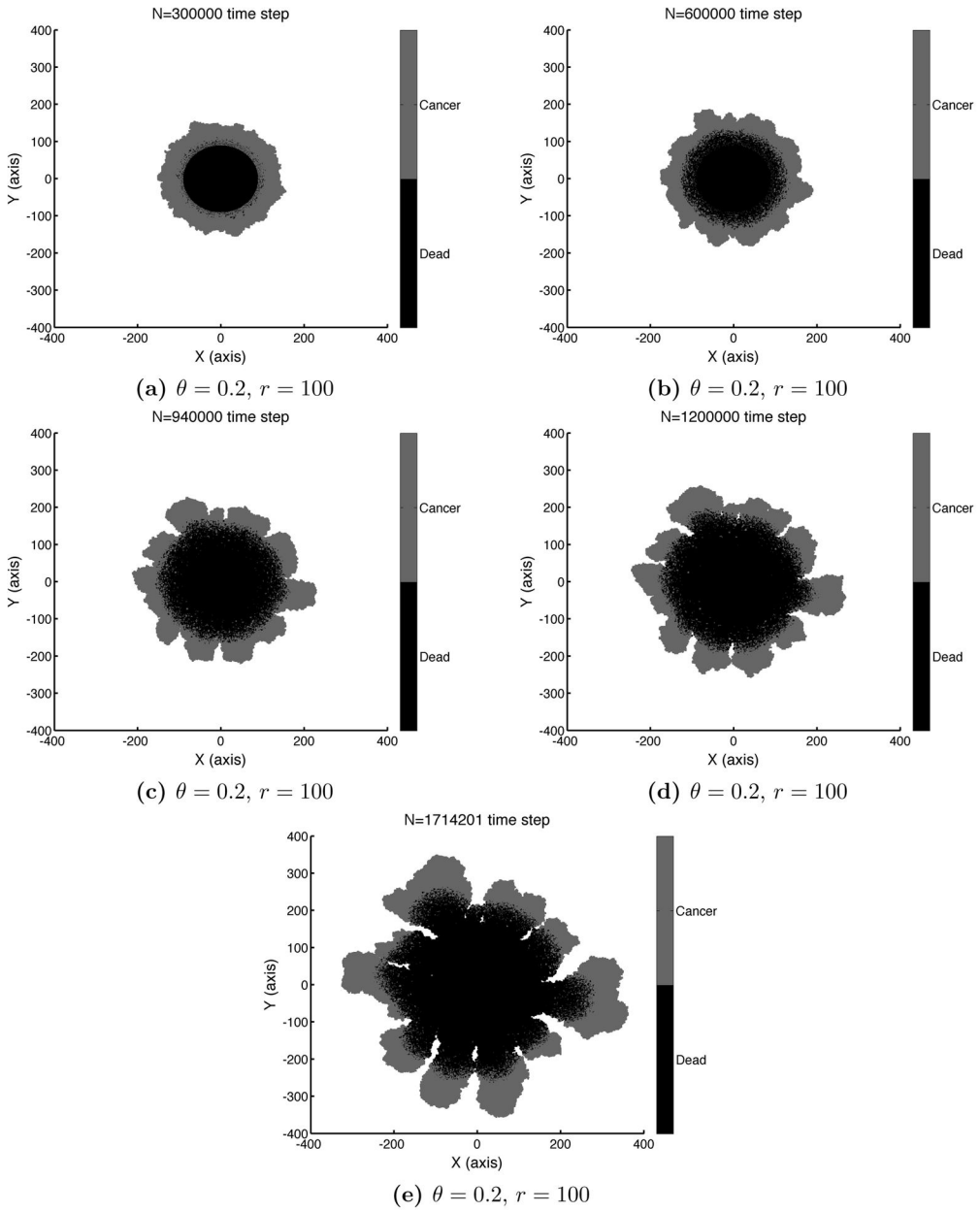

(a) $\theta = 0.2,\ r = 100$ (b) $\theta = 0.2,\ r = 100$

(c) $\theta = 0.2,\ r = 100$ (d) $\theta = 0.2,\ r = 100$

(e) $\theta = 0.2,\ r = 100$

Figure 7.

Simulation snapshots using the diffusive model on a 800 × 800 square stopped when the process has escaped the square with radius 720. We have started the simulation by using a ball of radius 100, with a thin layer of living cells on the periphery, located in the center of the domain Ω. Parameters and color scheme as in Figure 5.